DOI 10.1007/s11237-017-9498-6
Theoretical and Experimental Chemistry, Vol. 53, No. 1, March, 2017 (Russian Original Vol. 53, No. 1, January-February, 2017)

STRUCTURE, OPTICAL AND PHOTOCATALYTIC PROPERTIES OF ZnO/CuO/BENTONITE NANOCOMPOSITES IN THE OXIDATION OF 2,6-DICHLOROPHENOL

A. İ. Vaızoğullar

UDC 541.145

ZnO/CuO/bentonite (Bent) ternary nanocomposites were obtained by coprecipitation and characterized using FTIR spectroscopy, scanning electron microscopy (SEM), and X-ray diffraction (XRD). The SEM images indicate that the ZnO/CuO/Bent nanocomposites consist of ZnO nanorods and spherical CuO particles. The highest photocatalytic activity in the oxidation of 2,6-dichlorophenol (DCP) was found for the Zn_8Cu_1Bent nanocomposite. The trapping method was used to study the intermediates formed during the photoreaction. The major oxidizing agents of DCP are photogenerated h^+ valence band holes and $O_2^{\cdot-}$ radicals. The stable intermediates formed in the photochemical oxidation of DCP were characterized using high-resolution mass spectrometry.

Key words: *ZnO/CuO, bentonite, phenol, high-resolution mass spectrometry.*

Metal oxide semiconductors such as ZnO, Fe_2O_3, CuO, and TiO_2 have recently been commonly used as photocatalysts for various redox reactions [1]. ZnO is one of the most popular such photocatalysts in light of its high photosensitivity, low cost, and ready availability [2]. As a rule, nanoparticles (NP) of ZnO are hybridized with NP of noble metals or coupled with other semiconductors, in particular, CuO and TiO_2, to give highly-active photocatalysts [3]. Furthermore, zeolites and clays with a well-developed surface have been used as supports to further enhance the photocatalytic activity of ZnO [4]. Deposition on the support is often accompanied by a shift in the range of photosensitivity of the photocatalysts toward longer wavelengths, inhibition of the electron–hole recombination, and enhanced adsorption of the organic substrate molecules, which, on the whole, leads to a significant increase in photoactivity.

Cupric oxide CuO is a *p*-type semiconductor with a relatively narrow band gap [5], which permits its use upon coupling in composites with broad-band materials such as TiO_2 and ZnO [6]. Bentonite (Bent) clay has a large specific surface area, good adsorption characteristics, and can be combined with ZnO and CuO to obtain efficient photocatalysts [7]. Some workers have noted that bentonite can lead to extension of the spectral region of the light sensitivity of the photocatalyst attached to the surface of this support to the visible region and greater adsorption of phototransformation substrates [8]. In the present work, ZnO-CuO/Bent ternary composites were obtained by coprecipitation. The composites were characterized by FTIR spectroscopy, scanning electron microscopy (SEM), and X-ray diffraction (XRD) as well as BET adsorption measurements. The nanocomposites were found to display photocatalytic properties in the oxidation of toxic 2,6-dichlorophenol (DCP) by the

Medical Services and Techniques Department, Vocational School of Health Services, Muğla Sıtkı Koçman University, Muğla, Turkey. E-mail: aliimran@mu.edu.tr. Translated from Teoreticheskaya i Éksperimental'naya Khimiya, Vol. 53, No. 1, pp. 31-38, January-February, 2017. Original article submitted September 19, 2016; revision submitted November 11, 2016.

TABLE 1. Physicochemical Properties of the Photocatalyst Composites and Rate Constants for the Photooxidation of DCP

Photocatalyst	S_{BET}, m^2/g	Pore diameter, nm	Pore volume, cm^3/g	$I_{(002)}/I_{(100)}$	Band gap, eV	Mean NP diameter, nm	$k \cdot 10^{-3}$, min^{-1}	R^2
Bentonite	112.4	15.58	1.568	–	–	–	–	–
Zn_8Cu_1	5.22	11.52	0.016	0.791	3.24	51.8	23	0.86
Zn_4Cu_5Bent	4.02	24.8	0.025	0.887	3.23	20.4	19	0.93
Zn_6Cu_3Bent	3.77	11.4	0.013	0.559	3.25	41.8	16	0.92
Zn_8Cu_1Bent	11.77	31.8	0.098	0.801	3.26	19.7	39	0.99

action of UV light. The role of bentonite in this photoreaction was discussed and the conditions, under which the composites display highest activity, were established.

EXPERIMENTAL

A series of ZnO-CuO/Bent samples with different contents of ZnO-CuO (80, 60, and 40 mass %) as well as a ZnO-CuO binary composite were obtained by coprecipitation using copper acetate, zinc acetates, and bentonite. The solid particles obtained were washed thrice with water, dried at 80 °C, and calcined at 600 °C for 4 h. The samples were designated as Zn_8Cu_1Bent, Zn_6Cu_3Bent, Zn_4Cu_5Bent, and Zn_8Cu_1.

The phase composition of the samples was studied using a Rigaku Dmax 350 diffractometer with CuK_α radiation ($\lambda = 0.154056$ nm). The IR spectra were taken on a Thermo-Scientific Nicolet IS10-ATR FTIR spectrometer. The morphology of the sample particles was studied using a JEOL JSM-7600F scanning electron microscopy. The elemental composition of the samples was determined by energy dispersive X-ray (EDAX) spectroscopy. The Brunauer–Emmett–Teller (BET) adsorption/desorption isotherms for nitrogen, pore volume, and pore size of the samples were measured at 77.35 K using a Micromeritics Instrument Corporation ASAP 2010 instrument manufactured in the USA. The intermediates in the photocatalytic decomposition of DCP were determined by electron spectroscopy in combination with high-resolution mass spectrometry (HRMS) using a Shimadzu 1601 UV-Vis spectrophotometer combined with a Waters SYNAPT G1 mass spectrometer (ESI-TOF-MS) in the range 50-1000 Da. The desolvation temperature was 250 °C and the capillary voltage was 2 kV.

The diameter of the crystallites was evaluated using the Scherrer equation

$$d = B\lambda/\beta_{1/2}\cos\theta \quad (1)$$

where d is the mean particle diameter in the sample, B is the Scherrer constant (0.91), λ is the X-ray radiation wavelength, and $\beta_{1/2}$ is the full width at half-height of the diffraction maximum at diffraction angle θ. The physical characteristics of the nanocomposites obtained are summarized in Table 1.

RESULTS AND DISCUSSION

The IR spectra of the composites show a broad band with maximum at 430-440 cm^{-1}, which may be assigned to vibrations of the Zn–O bonds [5]. The maxima at 1600 and 3430 cm^{-1} correspond to vibrations of bonds in the water molecules

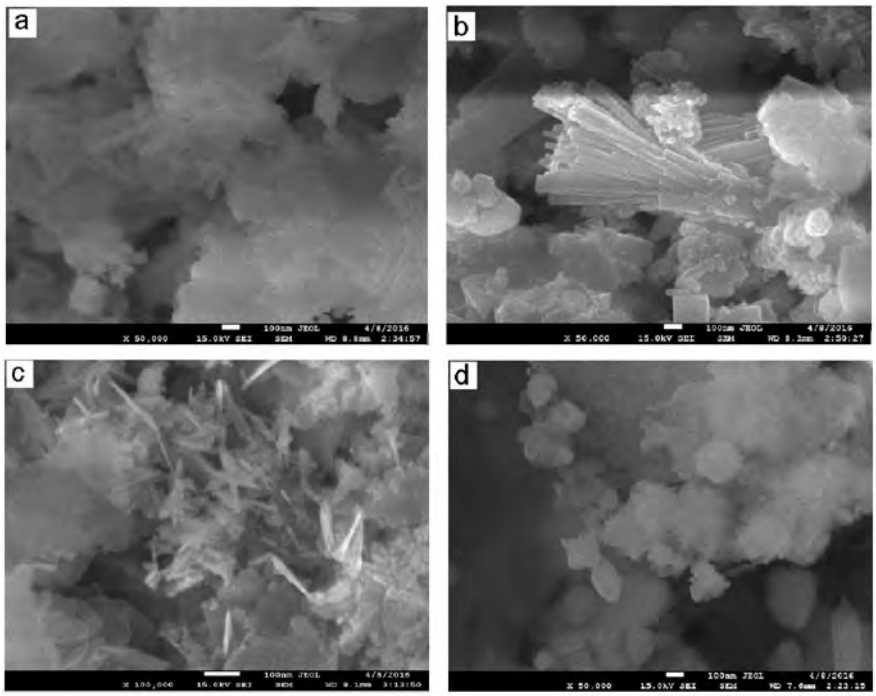

Fig. 1. SEM images of samples of Zn_4Cu_5Bent (a), Zn_6Cu_3Bent (b), Zn_8Cu_1Bent (c), and Zn_8Cu_1 (d).

TABLE 2. Ionized Fragment *m/z* Values, Exact Mass [M–H] and Proposed Structure of Intermediates (from HRMS data)

Sample	Fragment ions, *m/z*	Exact mass [M–H]	Proposed molecular formula
Fig. 6b	175, 176, 177, 178	[M–H]	$C_6H_2O_2Cl_2$
Fig. 6c	96, 97, 98, 100, 102, 114, 115	[M–Cl_2], [M–OCl],	C_6H_6O, $C_4H_4O_4$
Fig. 6d	96, 97, 98, 100, 102, 114, 115	[M–Cl_2], [M–OCl]	C_6H_6O, $C_4H_4O_4$

[9]. The bands at 1010 cm^{-1} (Si–O bond in-plane stretching vibrations) and 879 cm^{-1} (Al–Fe–OH fragment) are characteristic for bentonite clay [10]. The band at 1778 cm^{-1} is atributed to vibrations of the acetate anion bound to a Cu^{2+} ion [11]. The peaks at 539-850 cm^{-1} were assigned to vibrations of the Cu–O and Zn–O bonds in the corresponding oxides [12].

The morphology of the samples was studied by scanning electron microscopy. Microphotographs of Zn_4Cu_5Bent, Zn_6Cu_3Bent, Zn_8Cu_1, and Zn_8Cu_1Bent are given in Fig. 1. These images indicate that the samples contain a mixture of nanoparticles (NP) of two clearly different sizes. The aggregates of spherical NP correspond to the cupric oxide (Fig. 1, a-c), while zinc oxide is present as randomly-distributed short nanorods with mean diameter ~40 nm and length ~500 nm. Figure 1b shows that the ZnO nanorods in the Zn_6Cu_3Bent sample form a stratum structure with mean diameter ~100 nm and length ~600 nm. The nanorods in Zn_8Cu_1Bent decreases by ~100 nm (Fig. 1c), indicating an effect of the CuO additive on the morphology of the zinc oxide phase [13]. The Zn_8Cu_1 sample without bentonite shown in Fig. 1d has nearly spherical aggregates, indicating the structure-forming role of bentonite in the synthesis of these ternary composite catalysts.

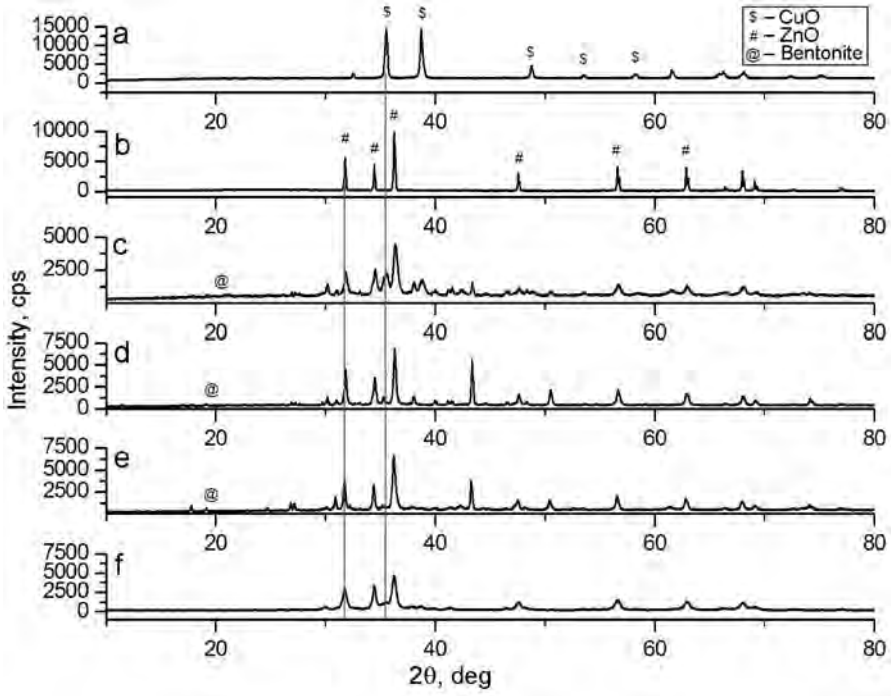

Fig. 2. XRD spectra for CuO (a), ZnO (b), Zn_4Cu_5Bent (c), Zn_6Cu_3Bent (d), Zn_8Cu_1 (e), and Zn_8Cu_1Bent (f).

The XRD diffraction peaks for ZnO, CuO, Zn_4Cu_5Bent, Zn_6Cu_3Bent, Zn_8Cu_1Bent, and Zn_8Cu_1 are shown in Fig. 2. The observed diffraction peaks are in accord with JCPDS No. 36-1451 (for ZnO) and No. 89-5899 (for CuO). In particular, the peaks at 31.8° (100), 34.5° (002), 36.3° (101), 47.5° (102), and 56.5° (110) are assigned to hexagonal ZnO (JCPDS No. 36-1451) (Fig. 2a, c-f) [14]. The diffraction peaks at 35.4° (002), 38.8° (111), 46.4° (11–2), 48.7° (20–2), and 53.6° (020) indicate the presence of monoclinic CuO (JCPDS No. 89-5898) (Fig. 2b-f). The characteristic bentonite peaks are found at 19.3° and 21.1° (Fig. 2c-e). Increasing the zinc oxide content leads to a corresponding increase in the ZnO reflections and decrease in the peaks characteristic for CuO (Fig. 2c-e) down to the virtual disappearance of these peaks for Zn_8Cu_1Bent (Fig. 2e). On the other hand, the diffraction pattern for Zn_6Cu_3Bent shows narrow peaks (Fig. 2d), while diffraction peaks for Zn_4Cu_5Bent and Zn_8Cu_1Bent are somewhat broadened (Fig. 2c,e). This finding may be attributed to the concurrent decomposition of $Zn(OH)_2$ and copper acetate during the calcination process [11] as well as the circumstance that most of the copper atoms in Zn_4Cu_5Bent and Zn_8Cu_1Bent are found in the ZnO wurtzite lattice [14]. Furthermore, the slight shift in the position of the diffraction peaks indicates change in the lattice parameters upon increasing the CuO content due to intimate contact between the ZnO and CuO phases [15].

The particle size in the samples obtained was calculated using Eq. (1) as well as the peak intensities and full-width at half maximum (FWHM) values in the corresponding XRD spectra (Table 1).

The BET surface areas of the heterostructures studied are given in Table 2. The specific surface area of the samples varied in the range from 3.77 to 11.77 m^2/g. The largest BET surface area was found for the Zn_8Cu_1Bent catalyst. On the other hand, the surface area of untreated bentonite is ~112 m^2/g. The smaller surface area for the ternary heterostructures indicates that they are blocked by deposited ZnO-CuO NP (Table 1). The specific surface area of the ternary composites increases with increasing ZnO content, which is attributed to the porosity of the zinc oxide phase. The pore volume of the composites also increases with increasing ZnO/CuO ratio, which indicates partial occupation of the ZnO pores by CuO [16].

A specially designed reactor with a UV light source consisting of a set of six 20-W Philips UV lamps emitting at $\lambda = 254$ nm placed 15 cm from the reaction mixture was used to study the photocatalytic process. The reaction was carried at atmospheric pressure and room temperature. An aqueous solution of 10 mg/L DCP was freshly prepared. A 0.1-g sample of the

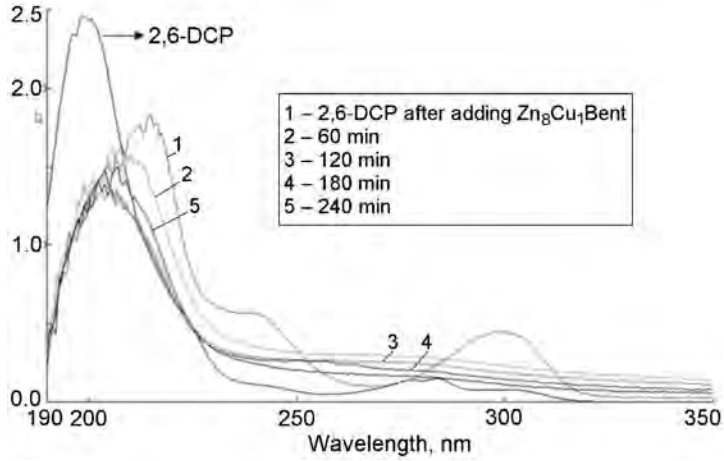

Fig. 3. Absorption spectra of the solution of 2,6-DCP obtained during the photocatalytic oxidation with the Zn_8Cu_1Bent composite.

photocatalyst was dispersed in 50 mL DCP solution and maintained with stirring for 60 min in order to establish the adsoption/desorption equilibrium. After turning on the irradiation, 1-mL probes of the solution were taken every 60 min and the concentration of DCP was determined spectrophotometrically. The conversion of DCP (X, %) was calculated as

$$X = \frac{C_0 - C}{C_0} \cdot 100 = \frac{A_0 - A_t}{A_t} \cdot 100 \quad (2)$$

where A_0 and A_t are the initial and current optical densities of the DCP solution at 298 nm, which, according to the Lambert–Beer law, are directly proportional to the initial C_0 and current DCP concentrations C [17]. The photocatalytic experiments were carried out in aqueous media at natural pH.

Absorption spectra of the absorption mixture at various moments during the photoreaction in the presence of Zn_8Cu_1Bent are shown in Fig. 3. These data show that the irradiation of a mixture of DCP and a photocatalyst leads to the appearance of new bands with maxima at 215 and 298 nm attributed to the formation of intermediates in the oxidation of DCP containing other chromophore groups, in particular, chlorohydroquinones and chlorocatechols. These bathochromic and hypsochromic shifts indicate a tight electronic interaction of DCP and the products of its decomposition with the photocatalyst surface [18]. The latter effect leads to an apparent increase in the phototransformation substrate concentration [19]. These spectral changes are characteristic for all the nanocomposites studied but are seen more clearly with increasing ZnO/CuO ratio. The highest photocatalytic activity was found for Zn_8Cu_1Bent. The most likely intermediates in the decomposition of DCP are chlorohydroquinones. C–Cl chromophores display a band at 270-325 nm attributed to n–π* transitions [19]. Figure 3 shows that the intensity of the band for the C–Cl chromophore at 270–325 nm decreases during the irradiation, indicating consumption of this intermediate. After 60 min irradiation, a band appears at 190-230 nm in the absorption spectrum, which may be assigned to π–π* transitions in aromatic fragments of DCP oxidation products. Upon further irradiation, the intensity of absorption in this spectral range increases somewhat, apparently due to the formation of various intermediates of smaller molecular mass, in particular, maleates.

The edge of the conductance band of CuO and ZnO is found at –4.96 and –4.19 eV, respectively, while the edge of the valence band is located at 3.26 and 0.99 eV, respectively [20]. Photoinduced electron transfer from the valence band to the conductance band occurs upon UV irradiation of the heterostructures in both semiconductors. Then, due to the more negative potential of the conductance band, electrons transfer from the conductance band of CuO to the conductance band of zinc oxide. Concurrently, the transfer of photogenerated holes from the valence band of ZnO to the corresponding band of CuO is possible

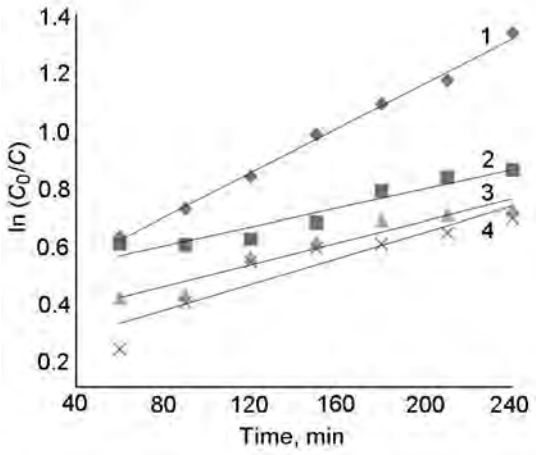

Fig. 4. Kinetic curves for the photocatalytic oxidation of 2,6-DCP in the presence of various composites: 1) Zn_8Cu_1Bent, 2) Zn_6Cu_3Bent, 3) Zn_4Cu_5Bent, 4) Zn_8Cu_1.

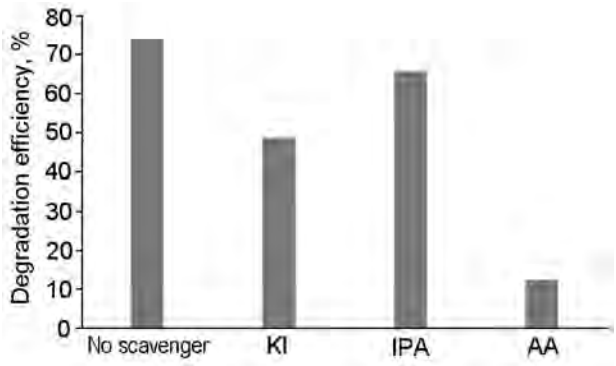

Fig. 5. Effect of traps for short-lived intermediate on the efficiency of the photodegradation of 2,6-DCP in the presence of Zn_8Cu_1Bent.

[21]. These transfers result in the irreversible spatial separation of the photogenerated charge carriers between the components of the ZnO-CuO heterostructures.

Figure 4 gives kinetic curves for the photocatalytic oxidation of DCP. The curves are linear when plotted for a pseudo-first-order reaction ln (C_0/C) vs. t, which permits us to calculate the effective rate constants of the photoreaction k, min^{-1}, from the tangent of the slope of these lines (Table 1).

Table 1 shows that the effective photoactivity of Zn_8Cu_1Bent is almost twice as high as for composites Zn_8Cu_1, Zn_6Cu_3Bent, and Zn_4Cu_5Bent, which may be attributed to greater surface activity of Zn_8Cu_1Bent as well as more efficient spatial separation of the photogenerated charge carriers. The rate of charge diffusion is known to depend on the pore volume of materials, and samples with greater pore volume have lower diffusional resistance, which may enhance the photocatalytic process in the case of Zn_8Cu_1Bent. The Zn_8Cu_1Bent composite has enhanced porosity, which provides for a larger number of active sites for adsorption and transformations of DCP as well as facilitating diffusion of the substrate to the surface of the ZnO-CuO active phase [22]. These results suggest a significant effect of the morphology of the bentonite nanocomposites on the course of photocatalytic reactions of their surface. In addition, the Zn_8Cu_1Bent sample has a higher ratio of intensities of the diffraction peaks corresponding to the polar and nonpolar ZnO faces, $I_{(002)}/I_{(100)} \geq 0.73$, which also may contribute to the enhanced photoactivity of this composite [23].

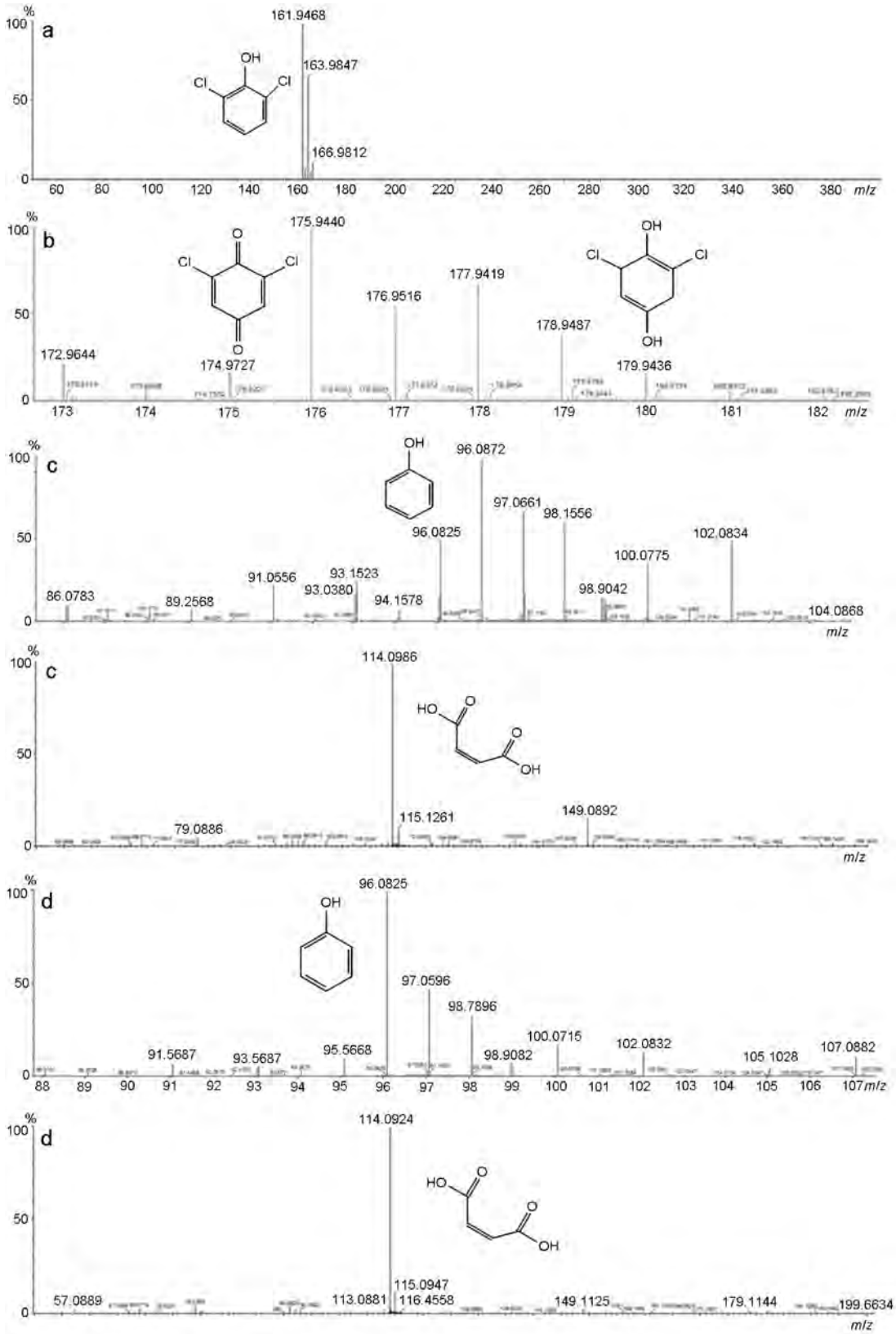

Fig. 6. High-resolution mass spectral data for samples of 2,6-DCP (a), 2,6-DCP in contact with the photocatalyst (b), and photocatalytic reaction products after 60 (c) and 240 min irradiation (d).

Comparison of the kinetic characteristics of the photoprocess found for Zn_8Cu_1 and Zn_8Cu_1Bent permits us to evaluate the role of bentonite in the photocatalytic reaction studied (Table 1). Zn_8Cu_1 was found to have lower photoactivity than the ternary Zn_8Cu_1Bent composite, which is most likely due to the greater specific surface area and adsorption ability of the ternary sample [24].

In order to elucidate the mechanism of this photocatalytic reaction, a series of experiments was carried out with traps for short-lived intermediates, which may be formed on the surface of the irradiated Zn_8Cu_1Bent composite ($OH^{\bullet}$, h^+, and $O_2^{\bullet-}$). In particular, 2-propanol, KI, and ascorbic acid (AA) were used to trap the hydroxyl radical, valence band holes, and superoxide radicals, respectively [25]. The data in Fig. 5 indicate that the photocatalytic conversion of DCP without added traps is 73.1% for Zn_8Cu_1Bent. This value in the presence of KI drops to 48.6%. On the other hand, added 2-propanol has virtually no effect on the efficiency of the photoreaction (65.8%). In the presence of AA, the photocatalytic activity of Zn_8Cu_1Bent is suppressed and the conversion of DCP is reduced to 12.4% after 240 min irradiation. Thus, the valence band holes h^+ and superoxide radical-anions $O_2^{\bullet-}$ act as the most active intermediates participating in the photocatalytic oxidation of DCP on the surface of Zn_8Cu_1Bent.

In order to determine the structure of stable intermediates in the photocatalytic oxidation of DCP, we used high-resolution mass spectrometry. Figure 6 gives the HRMS data for starting DCP, DCP in contact with the photocatalyst, and the reaction mixture taken 60 and 240 min after the onset of irradiation. The amount of individual fragments detected in the reaction mixture decreases as the photoreaction progresses. Similar products of the decomposition of DCP are present in the samples obtained after 60 and 240 min irradiation. The peak for m/z = 114.1 corresponds to maleic acid (Fig. 6c,d, Table 2). The peak for m/z = 96.1 corresponds to the loss of two chlorine atoms from the substrate (Fig. 6c,d, Table 2). The presence of smaller organic residues indicates extensive photocatalytic degradation of DCP on the surface of Zn_8Cu_1Bent (Fig. 6c,d), which is in accord with the electronic absorption results.

Thus, ZnO-CuO/bentonite composites were obtained by coprecipitation and found to display photocatalytic activity in the oxidation of 2,6-dichlorophenol in aqueous solution. The samples were characterized by XRD, SEM, and BET adsorption measurements. The SEM results indicated that the morphology of these composites depends significantly on the Zn/Cu ratio.

A number of photoreaction products were found using electronic spectroscopy and HRMS. DCP was found to convert upon UV irradiation into derivatives of hydroquinone and other phenolic intermediates, which undergo further degradation to give carboxylic acids and their derivatives. The highest photocatalytic activity was found for the Zn_8Cu_1Bent composite.

This work was carried out with the support of a grant from Muğla Sıtkı Koçman University (Project No. 15/139).

REFERENCES

1. X. X. Xu, C. Randorn, P. Efstathiou, and J. T. S. Irvine, *Nat. Mater.*, **11**, 595-598 (2012).
2. H. Xu, T. Yu, and J. Liu, *Mater. Lett.*, **117**, 263-265 (2014).
3. C. Wang, J. C. Zhao, X. M. Wang, et al., *Appl. Catal. B*, **39**, 269-279 (2012).
4. H. B. Hadjltaief, M. B. Zina, M. E. Galves, and P. D. Costa, *J. Photochem. Photobiol. A*, **315**, 25-33 (2016).
5. E. D. Sherly, J. J. Vijaya, and L. J. Kennedy, *Chin. J. Catal.*, **36**, 1263-1272 (2015).
6. T. Witoon, T. Permsirivanich, and M. Chareonpanich, *Ceram. Int.*, **39**, 3371-3378 (2013).
7. S. C. Motshekga, S. S. Ray, M. S. Onyango, and M. N. Momba, *J. Hazard. Mater.*, **262**, 439-446 (2013).
8. N. Saelim, R. Magaraphan, and T. Sreethawong, *Energy Convers. Manage.*, **52**, 2815-2818 (2011).
9. C. H. Ashok, K. Venkateswara Rao, and C. H. Shilpa Chakra, *J. Adv. Chem. Sci.*, **2**, 223-226 (2016).
10. C. Paluszkiewicz, M. Holtzer, and A. Bobrowski, *J. Mol. Struct.*, **880**, 109-114 (2008).
11. R. K. Sharma and R. Ghosen, *Ceram. Int.*, **40**, 10919-10926 (2014).
12. I. Y. Erdogan, *J. Alloys Compd.*, **502**, 445-450 (2010).
13. R. Saravanan, B. Karthikeyan, V. K. Gupta, et al., *Mater. Sci. Eng. C*, **33**, 91-98 (2013).
14. L. Chow, O. Lupana, G. Chai, et al., *Sensors Actuators*, **189**, 399-408 (2013).
15. M. H. Habibi and B. Karimi, *J. Ind. Eng. Chem.*, **20**, 925-929 (2014).

16. V. Agarwal, S. Patel, and K. K. Pant, *Appl. Catal. A*, **279**, 155-164 (2005).
17. A. Shirzadi and A. B. Ejhieha, *J. Mol. Catal. A*, **411**, 222-229 (2016).
18. E. M. Seftel, M. C. Puscasub, M. Mertens, et al., *Appl. Catal. B*, **150**, 157-166 (2014).
19. J. S. Valente, F. Tzompantzi, and J. Prince, *Appl. Catal. B*, **102**, 276-285 (2011).
20. Y. Xu and M. A. A. Schoonen, *Am. Miner.*, **85**, 543-556 (2000).
21. S. Q. Wei, Y. Y. Chen, Y. Y. Ma, and Z. C. Shao, *J. Mol. Catal. A*, **331**, 112-116 (2010).
22. L. Pinho and M. J. Mosquera, *Appl. Catal. B*, **134/135**, 205-221 (2013).
23. C. M. Pedrero, H. Silva, D. A. Pacheco, et al., *Appl. Catal. B*, **174**, 67-76 (2015).
24. N. R. Reyna, L. H. Reyes, J. L. G. Jorge Mar, et al., *Photochem. Photobiol. Sci.*, **12**, 653-659 (2013).
25. H. Gan, G. Zhang, and H. Huang, *J. Hazard. Mater.*, **250/251**, 131-137 (2013).